The Zeeman Effect in Mercury Vapor and the Determination e/m by Fabry-Perot Interferometry

Edwin Ng*
MIT Department of Physics
(Dated: March 17, 2012)

We analyze the Zeeman fine structure of mercury vapor by high-resolution spectroscopy using a Fabry-Perot interferometer. We use the 5460.7 Å green line and the 5769.6 Å yellow line of mercury, in fields up to approximately 11.7 kG and 6.3 kG, respectively. By comparing our measurements against the vector model of the Zeeman effect, we determine the ratio $e/m = (1.813 \pm 0.130_{\text{rand.}} \pm 0.076_{\text{syst.}}) \times 10^{11}$ C/kg. Polarization of the fine structure lines is observed, and hyperfine structure can also be resolved on the green line. We include a detailed discussion on the calibration of the Fabry-Perot cavity length.

I. INTRODUCTION AND THEORY

The broadening of atomic spectral lines in the presence of a magnetic field was first observed by Pieter Zeeman in 1897, indicating the presence of a charged, massive particle in the atom. Soon after, the effect was shown to arise from the interaction of the electron with the magnetic field, causing its excitation levels to split in energy.[1]

This so-called fine structure involves splittings on the order of 0.1 Å for fields around 10 kG. To perform such high resolution spectroscopy, we use in this experiment a scanning Fabry-Perot (FP) interferometer, pioneered by by Charles Fabry and Alfred Pérot, also in 1897.

I.1. The Zeeman Effect

In the context of modern quantum mechanics, the Zeeman splittings of an atomic spectral line arises from lifting the degeneracy within the two energy levels of that transition, by introducing an integral magnetic quantum number m_j associated with J_z, the component of the electron's angular momentum in the direction of the field.

Because the electron has both orbital and spin angular momentum, we simplify our analysis by appealing to the vector model of angular momentum. For an electron with angular momenta numbers l (orbital), $s = 1/2$ (spin), and j (total), we define the Landé g-factor

$$g = 1 + \frac{j(j+1) + s(s+1) - l(l+1)}{2j(j+1)}$$

In the vector model, j and therefore g are determined by l, while $m_j \in [-j, j]$. The energy of an electron with a given m_j and g is $E = \mu_0 g B m_j$, where $\mu_0 = e\hbar/2m$ is the Bohr magneton and B is the applied field. A diagram of the green line of mercury is shown in Figure 1.[2]

From the energy level diagram, we can calculate the energy difference $\delta\varepsilon$ between any two lines in units of $\mu_0 B$. For the green line, the splitting within each selection group is 1/2, while the splitting between middle-π and middle-σ is 3/2.

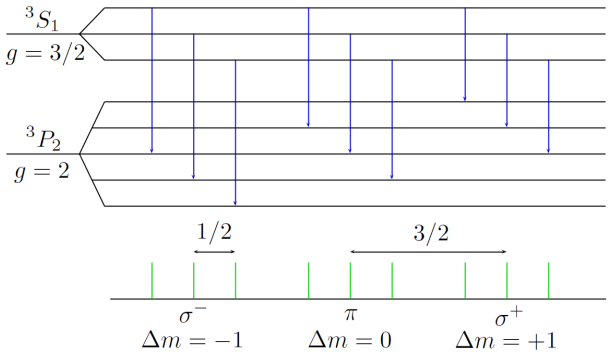

FIG. 1. An energy level diagram of the 5460.7 Å green line of mercury, corresponding to the transition $^3S_1 \to {}^3P_2$. The energies on the bottom spectrum are in units of $\mu_0 B$.

We can draw a similar energy level diagram for the yellow doublet lines. For the transition at 5769.6 Å ($^3D_2 \to {}^1P_1$), these splittings are 1/6 and 7/6, while for the transition at 5790.7 Å ($^1D_2 \to {}^1P_1$), they are 0 and 1 (hence its spectrum only has three lines).

I.2. The Fabry-Perot Interferometer

The Fabry-Perot interferometer consists of two parallel partially-transmitting mirrors separated by a cavity length L. When light of wavelength λ enters through one mirror, interference occurs within the cavity. Since the path separation depends on the angle θ at which the light leaves, relative to the axis of the beam, the interference equation for the FP is $2L\cos\theta = m\lambda$ for m an integer. When correctly aligned, the output of the FP are concentric rings, with m increasing by radius.

The angular separation $\Delta\theta$ between two modes is the free spectral range (FSR) of the cavity; it determines the range of wavelengths that fits into one mode. If we send in light of wavelengths λ and $\lambda+\delta\lambda$ (for example, two fine structure lines), we see a corresponding angular splitting $\delta\theta$. It can be shown[1] that

$$\delta\lambda = \frac{\lambda^2}{2L}\left(\frac{\delta\theta}{\Delta\theta}\right) \tag{1}$$

where $\cos\theta = 1$ near the axis of the beam.

* ngedwin@mit.edu

We now relate the energy of a splitting to the output of the FP. Let $R = \delta\theta/\Delta\theta$ be the ratio of the optical splitting against the FSR. The energy separation between wavelengths λ and $\delta\lambda$ is $\delta E = (hc/\lambda^2)\delta\lambda$. Setting this equal to $\mu_0 B\delta\varepsilon$ (from Zeeman theory) and using Equation 1 to eliminate λ (from FP theory), we find

$$\frac{R}{\delta\varepsilon} = \frac{e}{m}\left(\frac{L}{2\pi c}\right)B \tag{2}$$

This is the governing equation for this experiment. We vary B and measure $R/\delta\varepsilon$ for the corresponding splittings; the resulting linear relation yields e/m.

II. EXPERIMENTAL SETUP

The setup of the experiment is shown schematically in Figure 2. All apparatus except for the magnet and lamp are fixed to an optical table.

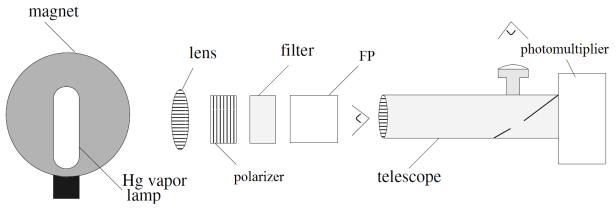

FIG. 2. A schematic of the experimental setup. Visual monitoring of signal occurs at the output of the FP and the eyepiece of the telescope. Adapted from [1].

The source is an Oriel mercury vapor lamp powered by a 20 mA DC power source and covered by a cap with an aperture of about 1 cm^2. The lamp is placed between two moveable pole pieces of an electromagnet, powered by a Sorenson SRL supply delivering a maximum of 35 A and cooled by chilled water to prevent overheating.

The light passes through a collimating lens, with a focal length of 400 mm. A narrow-band interference filter at 5470 Å or 5700 Å (for green and yellow, respectively) is located approximately 10.5 cm from the lens, and a removable polarizer is placed in between to differentiate between σ and π lines.

The Fabry-Perot interferometer (by Burleigh) is located 12 cm behind the filter, and the base of the FP is about 40.5 cm (with optical axis 102 mm). The left mirror is fixed and its position is indicated by a vernier, while the right mirror is controlled three micrometers (with precision 5 µm, for coarse control of the cavity length and to adjust for parallelism. We use the micrometer closest to the edge of the optical table to set the length and adjust the other two to align. For our measurements, the left mirror is fixed at (23.7 ± 0.1)mm, while the micrometers are set as needed to optimize the FSR.

The telescope, focused at infinity, is located about 39 cm from the output of the FP, to allow enough space for visual monitoring of the FP. The telescope contains a mirror with a laser-drilled hole, which allows a fixed point in the optical field to pass to a photomultiplier for signal detection. The interference spectrum is obtained by sweeping the length of the FP in the hundredths of nm range and monitoring the signal detected by the photomultiplier. We find it is useful to place the pinhole onto the bright image of the lamp, to amplify the signal.

The photomultiplier is biased at 950 V by a Bertan 313B HV power supply, and its output is fed into a Princeton 113 pre-amplifier, set to 2K gain with a high-pass filter at 3Hz. We then send the signal into an Agilent 54621A oscilloscope to obtain the interferogram.

The scanning is performed by a Burleigh RC-44 programmable ramp generator, which controls three piezoelectric crystals to sweep the FP cavity length. The available controls are the individual biases on the three crystals, an overall ramp bias (to adjust starting position), a ramp amplitude (to adjust modes per sweep), and a ramp duration switch (to control speed of ramping). We use a ramp duration of 200 ms × 100 for alignment, 1 s × 100 for measurements, and 500 ms × 100 for calibration. Trim controls are also available on each crystal, but we do not use them and set them to the zero position.

III. OBSERVATIONS AND MEASUREMENTS

III.1. Hyperfine Structure ($B = 0$)

Even in the absence of a magnetic field, the high resolution of the Fabry-Perot should allow us to observe some hyperfine structure in the 5460.7 Å line, due to isotope effects.[2] An interferogram showing possible hyperfine lines is shown in Figure 3.

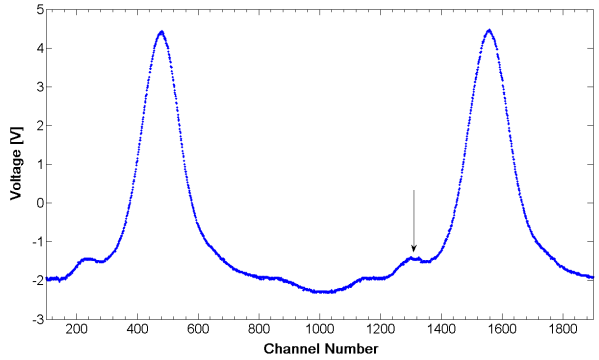

FIG. 3. An interferogram showing a hyperfine line of the Hg green line, with the isotope-201 line indicated by an arrow. The micrometer setting is (11.240 ± 0.005) mm.

One possible indication of hyperfine structure is the broadness of the main peak, beyond noises such as Doppler broadening and optical imperfections, which could be due to the effects of reduced mass in the even isotopes. However, clear evidence of this effect is impossible with the resolution we have here.

More unequivocal, however, is the faint line directly to the left of the main peak, which we have identified to be the isotope-201 line of mercury.[3] The energy of the transition in this odd isotope has been shifted due to magnetic dipole effects, where the field of the nonzero nuclear spin couples to the electron's motion. From a fitting procedure similar to that described in Section V, we find $R = 0.2347 \pm 0.0003$. However, we do not calculate $\delta\lambda$ because we are assuming the value in [3] and using this measurement for calibration (see Section IV).

III.2. Measurements with Applied B

Once the magnetic field is turned on, we visually observe clear indications of Zeeman splitting. To perform measurements, we use the rolling mode of the oscilloscope to record the signal through the pinhole for one ramp duration (100 s). At the end of the ramp, we stop the run and save the scope trace to disk for later analysis.

Since the ramping is linear and the oscilloscope samples at regular intervals (2000 points per trace), we will assume in our analysis that the distances on the interferograms are linearly related to the angular distance θ on the output of the FP. Thus, we measure R by measuring $\delta n/\Delta n$, where n is the scope trace sample index (labelled in our interferograms as "channel number").

The magnetic field is measured with a Hall effect gaussmeter probe, zeroed and calibrated against a standard 5 kG calibration magnet. We measure the field around the aperture of the lamp by rotating the probe until we obtain a maximum (so that the probe is perpendicular to the field lines), and we include the spatial variations in B into our uncertainties.

For the green line, we perform eight sets of measurements, with field strengths of (11.70 ± 0.03)kG, (11.20 ± 0.02)kG, (11.12 ± 0.05)kG, (10.90 ± 0.02)kG, (10.03 ± 0.02)kG, (8.21 ± 0.03)kG, (5.85 ± 0.05)kG, and (3.24 ± 0.02)kG. For the first six measurements, we obtain two interferograms with no polarizer applied, one with the polarizer at 0° (for σ lines) and one with the polarizer at 90° (for π lines). For the last two, we take only σ. A sample interferogram is shown in Figure 4.

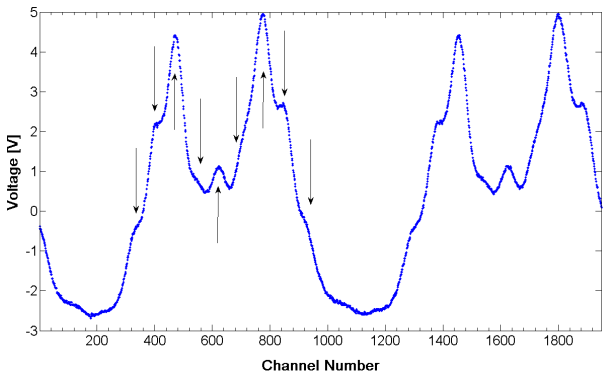

FIG. 4. A sample interferogram of Zeeman splitting of the mercury green line, at $B = (11.70 \pm 0.03)$kG with no polarizer. The arrows indicate the nine predicted lines of the spectrum.

For the yellow lines, we perform five sets of measurements, with field strengths of (6.32 ± 0.02)kG, (5.60 ± 0.03)kG, (5.04 ± 0.03)kG, (4.36 ± 0.01)kG, and (3.74 ± 0.02)kG. We use all three polarization settings for the first measurement, but because of time constraints, we take only full and σ for the rest.

The micrometer setting we use to obtain an optimal FSR are (10.660 ± 0.005)mm for the green line and (10.680 ± 0.005)mm for the yellow lines. In general, the other two micrometers are changed as necessary to align the mirrors; typically the one opposite the reference micrometer reads about 0.01 mm higher and the bottom one reads about 1 mm lower.

IV. CALIBRATION OF FP CAVITY LENGTH

As is evident from Equation 2, determination of the FP cavity length is crucial to the analysis of this experiment. Although the micrometers are precise to 5 µm, visual inspection of the FP cavity length is restricted by the precision of the vernier for the left mirror, which is precise to only 0.1 mm.

If the left mirror is fixed, the reading L' on the reference micrometer is related to the true length of the cavity by $L = L' - L_0$, where L_0 is the reading of the reference micrometer at zero cavity length. Rearranging Equation 1, the governing equation for calibration is

$$L' = \frac{\lambda^2}{2\delta\lambda} R + L_0 \tag{3}$$

We use the doublet lines of mercury for this calibration procedure. For the lengths L', we pick 10.610 mm, 10.620 mm, 10.630 mm, 10.640 mm, 10.660 mm, 10.690 mm, 10.700 mm, and 10.720 mm (with uncertainty 2.5 µm). To obtain R, we fit the inteferograms as described in Section V.

We do not, however, obtain a linear relation at first glance. The 20 Å separation of the two doublet lines are in fact much larger than the FSR can accomodate. Thus, between 10.690 mm and 10.700 mm, we observe that the two peaks "hop" past each other, and the value of R shifts by one multiple of the FSR. Taking this into account yields a very linear relationship.

However, because of this effect of "mode-hopping", we need to take $R \mapsto R + k$ in Equation 3 since the two lines do not come from the same mode. With $k = 0$, we get $L_0 = (10.603 \pm 0.002)$mm. However this is not true, since we can in fact turn the reference micrometer to this value and observe a nonzero cavity length. With this procedure, we are able to conclude $15 < k < 25$.

To further nail down the value of k, we turn to the hyperfine line. Since we know the value of $\delta\lambda_0$ from [3], we compute L_k for every k in this range by doing a linear fit for each one, and we use Equation 1 to compute the resulting $\delta\lambda_k$ of the hyperfine splitting. We then take the value of k that yields a minimum for $|\delta\lambda_k - \delta\lambda_0|$. We find, using this procedure, that $k = 19$ gives the correct number of mode hops between the two doublets, which yields $L_0 = (9.13 \pm 0.04)$mm.

V. ANALYSIS OF DATA

The relevant information in our interferograms is contained in the channel numbers n_j of each peak. From these channel numbers, we can compute the splitting δn between any two Zeeman lines, as well as the FSR Δn (using two identical lines from different modes).

For the purposes of fitting, we find the σ interferograms (polarizer at 0°) to be the most convenient to use for the green line. For the yellow line, we use the full interferograms (no polarizer) for the lowest two B fields, and σ again for the higher ones.

Note that we do not use the 5790.7 Å line of the yellow doublet. This is because it contains only three Zeeman lines from the coincidence of the Landé g factors for the transition, and this turns out to be insufficient data for our analysis technique.

V.1. Fitting Procedure

From Figure 4, one good choice of a fitting function would be the sum of a number of Gaussians on a constant offset. This is given by the functional form

$$y = b + \sum_j A_j \exp\left[-\frac{(x-n_j)^2}{2c_j^2}\right]$$

We perform a gradient search to fit the relevant portions of each interferogram to this general form and extract the values of n_j and its uncertainty from the fits. For the uncertainties in y, we use a constant 20 mV, which we find characterizes the local voltage fluctuations in the scope trace well.

V.2. Analysis with High B

For high values of B, we can observe and fit for all nine lines of the Zeeman splittings. We therefore use the following procedure for analyzing the resulting data, which applies to the green lines down to 5.04 kG.

We know, from Figure 1, that all nine lines are separated by $\delta\varepsilon = 1/2$ equally. Therefore, to obtain R, we first compute the splittings δn_j between *consecutive lines*. This gives us eight numbers, and since we expect them to be equal, we take δn to be their error-weighted average $\langle \delta n_j \rangle$, with a statistical uncertainty propagated from the uncertainty on each n_j.

Finally, we add to this uncertainty the systematic uncertainty of the uneven splittings (due possibly to our fitting procedure, or some physical effect); this is given by the standard deviation $\sigma[\delta n_j]$, divided by $\sqrt{8}$.

V.3. Analysis with Low B

For low values of B, however, we cannot fit for all nine lines of the Zeeman splittings. Rather, we only see two peaks, corresponding to σ^- and σ^+ (π is slightly noticeable, but it is not prominent enough to accomodate a fit). We therefore use the following procedure for analyzing the resulting data, which applies to the two lowest field interferograms for green, and to all of the yellow.

Since our fit returns n_j for only two peaks (and hence only a *single* δn), we must make an assumption about which lines these correspond to. For simplicity, we associate these with middle-σ^- and middle-σ^+. We then compute R directly from δn and Δn, which takes into account only the statistical uncertainties in n_j.

Because of this representation, however, we introduce systematic uncertainties in $\delta\varepsilon$. To account for this, we let the uncertainty in $\delta\varepsilon$ be the energy separation within each selection group. This gives $\delta\varepsilon = 3 \pm 1/2$ (for the green line) and $\delta\varepsilon = 14/6 \pm 1/6$ (for the yellow line).

V.4. Determination of e/m

The values of $R/\delta\varepsilon$ that result from the two analysis techniques above, after propagating the uncertainties correctly, are plotted against B for the green and yellow lines in Figure 5 below.

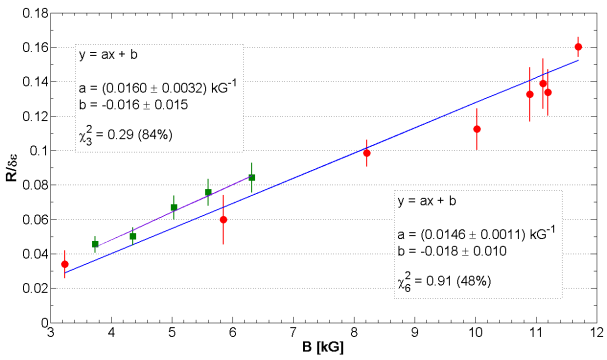

FIG. 5. Linear fits of $R/\delta\varepsilon$ against B for the 5769.6 Å yellow (top) and the green 5464.7 Å (bottom) Zeeman splittings. Note that the vertical offsets are small, as they should be, given Equation 2.

We derive e/m from the slope of the line using Equation 2. The value of e/m estimated from the green line fit is $(1.796 \pm 0.138) \times 10^{11}$C/kg, while the value of e/m from the yellow line fit is $(1.949 \pm 0.389) \times 10^{11}$C/kg. Taking the average of these two results and quoting half their difference as a lower bound on the systematic error, our best determination is $e/m = (1.813 \pm 0.130_{\text{rand.}} \pm 0.076_{\text{syst.}}) \times 10^{11}$ C/kg.

VI. CONCLUSIONS

Using the high resolution afforded by a Fabry-Perot interferometer, we are able to observe the Zeeman fine structure of mercury vapor produced by fields of tens of kG (and even some hyperfine structure). We verify many of the qualitative features of the Zeeman spectrum, including the presence of polarization and the relative splittings of each line.

From the interferograms, we arrive at an estimation of $e/m = (1.813 \pm 0.130_{\text{rand.}} \pm 0.076_{\text{syst.}}) \times 10^{11}\text{C/kg}$. We note that the accepted value of $e/m = 1.759 \times 10^{11}\,\text{C/kg}$; this is an error of about 3.1%. Compared to previous attempts at this important physical quantity (c.f., Relativistic Dynamics), this is our most accurate measurement to date.

[1] M.I.T. Junior Lab Staff, "The Zeeman Effect and Hyperfine Structure in Mercury," (2011).

[2] A. Melissinos, *Experiments in Modern Physics* (Academic Press, 1966).

[3] J. Sterner, "Interferometric measurements of the hyperfine structure of the green mercury line," Phys. Rev. **86** (1952).

ACKNOWLEDGMENTS

EN gratefully acknowledges his lab partner, Polnop Samutpraphoot, and the Junior Lab staff for their assistance in understanding the theory behind the design and analysis of this experiment.